International Journal of Heat and Fluid Flow 29 (2008) 1393–1401

Contents lists available at ScienceDirect

International Journal of Heat and Fluid Flow

journal homepage: www.elsevier.com/locate/ijhff

Computation of weakly ionized air flow in thermochemical nonequilibrium over sphere–cones

Ghislain Tchuen [a,*], David E. Zeitoun [b]

[a] Institut Universitaire de Technologie Fotso Victor, Université de Dschang, BP. 134, Bandjoun, Cameroon
[b] Ecole Polytechnique Universitaire de Marseille, Université de Provence, DME, 5 rue Enrico Fermi Technopole de Chateau Gombert, 13453 Marseille Cedex 13, France

ARTICLE INFO

Article history:
Received 15 November 2007
Received in revised form 17 June 2008
Accepted 19 June 2008
Available online 29 July 2008

Keywords:
Weakly ionized
Upwind solvers
RAM-C flights
Nonequilibrium flow

ABSTRACT

The weakly ionized high enthalpy flow in thermochemical nonequilibrium over blunt bodies at zero incidence is investigated. The numerical technique uses time dependent Navier–Stokes equations which relies on a multi-block finite volume scheme based on a second-order accurate Total-Variation-Diminishing. The convective flux terms are calculated by Riemann's solvers based on a MUSCL approach, and the viscous terms are discretized by second-order central difference. The flowfield is thermally characterized by multi-temperatures, and the correction of the speed of sound due to the electron translational temperature has been included. An evaluation of aerothermodynamics parameters is carried out for RAM-C flights (which is a 9° sphere–cone). A good comparison is shown with previous simulations and experimental data.

1. Introduction

The development of re-entry vehicle requires an accurate knowledge of hypersonic flows over blunt bodies and a better prediction of thermal protection system for extremely high temperature. The flowfield is characterized by a strong detached bow shock with a subsonic pocket in the nose region. The high kinetic energy content is converted to internal energy, thus increasing the temperature of the gas. The high gas temperature causes the significant excitation of the internal energy modes, the dissociation of diatomic molecules, and ionization. Under typical hypersonic condition, air must be considered as a plasma around the vehicle, which perturbes traditionally the communication between the vehicle and the ground control station because the plasma absorbs radio waves (Luneau and Rossines, 1978). The computation of such a flowfield is a challenging task.

Successful conception of such a high technology would be obtained after some knowledge of the thermochemical nonequilibrium phenomena, and how they affect the performance of the vehicle. More accurate results of heat transfer and thermodynamic properties can be obtained either from numerical simulation or with experimental facilities. The least expensive approach is the numerical prediction which is a reasonable alternative after sufficient validation. The objective of this research is to develop a method for predicting weakly ionized hypersonic flow over blunt bodies. The downstream region was of considerable interest, and the method could not be restricted to the stagnation region. This work points out the contribution of electronic excitation, ionized species and thermochemical coupling on aerothermodynamic parameters.

The computational results depend on the thermochemical model and the strategy of resolution. In the past, several authors have successfully investigated thermochemical nonequilibrium flow with ionization. To simplify the calculations, Palmer (1989), Gnoffo et al. (1989) used the two-temperature model in which the vibrational temperature is assumed to be equal to the electronic temperature. Candler and MacCormarck (1991) assumed that each molecule has their proper vibrational temperature, and developed a six-temperature model. However, Candler and MacCormarck (1991) concluded the same as Park (1990) that the use of one vibrational temperature is a reasonable approximation. Candler and MacCormarck (1991) and Josyula and Bailey (2003) used the same approach to obtain the electron temperature from an equation of the electron energy. Coquel and Marmignon (1997) assumed that thermal conductivity and viscosity of the electrons are negligible, and have found a conservative formulation for weakly ionized gas. Mitcheltree (1991) investigated the application of several dissociation and ionization models for high-velocity entries with a two-temperature model. All the authors cited above assume that the vibration–dissociation coupling is modeled according to the empirical relationship proposed by Park (1990), and all use air chemical model with seven species.

In this work, the gas is chemically regarded as a mixture of partially ionized air with seven species O, N, NO, O_2, N_2, NO^+, e^-. The chemical reactions model used in this paper is proposed by Park

* Corresponding author. Tel.: +237 99 93 04 89; fax: +237 33 01 46 01.
E-mail address: tchuengse@yahoo.com (G. Tchuen).

0142-727X/$ - see front matter Crown Copyright © 2008 Published by Elsevier Inc. All rights reserved.
doi:10.1016/j.ijheatfluidflow.2008.06.002

Nomenclature

$A_{i,j}$	area of the cell (i,j)
$C^s_{v,\mathrm{tr}}$	specific heat at constant volume for species s for translational energy
D_s	diffusion coefficient of species s
ρe_e, e_{e_s}	electron–electronic energy per unit volume, mass of species s
$\rho e_{\mathrm{v}_m}, e_{\mathrm{v}_m}$	vibrational energy per unit volume, mass of molecules m
F_k	convective and viscous fluxes in x and y directions on each side of the cell
$H_{i,j}$	axisymmetric source term
$\hat{M}_s$	molecular weight of species s
NM	total number of molecules
N_k	outward normal vector on each side of the cell
NS	total number of species
p_s	pressure of species s
$Q_{\mathrm{T-e}}$	translation–electronic energy transfer rate
$Q_{\mathrm{T-v}_m}$	translation–vibration energy transfer rate
$Q_{\mathrm{v}_m\mathrm{-e}}$	vibration–electronic energy transfer rate
$Q_{\mathrm{v-v}_m}$	vibration–vibration energy transfer rate
$r_{i,j}$	radius of the cell-center position
T	translational–rotational temperature
T_a	geometrically averaged temperature
T_e	electron–electronic excitation temperature
T_{v_m}	vibrational temperature of molecule m
t	time
U	vector of conserved quantities
u, v	velocity in x and y directions

Greek symbols

ϵ	electron charge
λ_tr	translational thermal conductivity of mixture
$\lambda_\mathrm{v,m}$	vibrational thermal conductivity of molecule m
λ_el	electronic thermal conductivity of mixture
ω_s	mass production rate for species s
γ	ratio of specific heat

species s

θ_r	characteristic temperature of reaction r
$\theta_\mathrm{v,m}$	characteristic temperature of vibration
ρ	total density
ρ_s	density of species s

Subscripts

eq	equilibrium
m	molecule
s	species
w	wall
∞	freestream

(1985) which is applied to seven air species with 24 elementary reactions. To couple the thermal and chemical nonequilibrium effects, the vibration–dissociation–vibration process has been taken into account with Park's model (1990). The flowfield is analyzed thermally by using a model with four temperatures. It is assumed that a single temperature controls the trans-rotational mode (T). The vibrational–vibrational coupling between the various molecules in nonequilibrium is taken into account, and two distinct temperatures are used for their vibrational energy ($T_{\mathrm{v}_{\mathrm{N}_2}}$, $T_{\mathrm{v}_{\mathrm{O}_2}}$). NO and NO^+ are assumed to be in thermodynamic equilibrium with the translational temperature. The last temperature is used for the electronic-free electron modes (T_e). The electron temperature is obtained from the electron–electronic energy which limits the numerical instabilities caused by the comparatively small mass of the electron. This can be a reasonable assumption because the difference between excitation temperature of the electronic mode and the electron temperature is not yet clearly defined. A good knowledge of the vibrational and electron temperature plays an important role in a high temperature gas because they improve the definition and evaluation of the chemical and physical properties of ionized hypersonic flowfield.

A robust flow solver has been developed based on the solution of time-dependent Navier–Stokes equations with ideal gas assumption. The code is based on a multi-block finite volume scheme using the upwing technology with Riemann algorithm replaced by an AUSM+ algorithm in the case of a strong shock wave. The MUSCL approach is used in conjunction with second-order total variation-diminishing (TVD) which accounts for nonequilibrium effects and ionization. The perfect gas relations are used to determine the thermodynamic relations. The modified speed of sound due to the presence of electron translational temperature is implemented in the flux-splitting procedure.

The various upstream flow conditions for these computations are equivalent to those obtained in the RAM-C flight. The numerical results presented in this paper have well been compared with experimental data and with those obtained numerically by other authors. Emphasis is placed on the influence of the nonequilibrium and ionization effects on the flowfield.

2. Analysis

The governing equations for weakly ionized flow in thermochemical nonequilibrium have been developed by Appleton and Bray (1964) and Lee (1985). The two-dimensional full laminar Navier–Stokes equations resolved in this work are written as conservation laws in differential form as follows:

One mass conservation equation for each species,

$$\frac{\partial \rho_s}{\partial t}+\frac{\partial \rho_s u_j}{\partial x_j}+\frac{\partial \rho_s V_s^j}{\partial x_j}=\omega_s. \tag{1}$$

A mass-average momentum equation in x and y directions,

$$\frac{\partial \rho u_i}{\partial t}+\frac{\partial(\rho u_i u_j+p\delta_{ij})}{\partial x_j}+\frac{\partial \tau_{ij}}{\partial x_j}=\sum_s \epsilon N_s Z_s E_i. \tag{2}$$

A total energy equation,

$$\frac{\partial \rho e}{\partial t}+\frac{\partial}{\partial x_j}((\rho e+p)u_j)+\frac{\partial}{\partial x_j}(q_{t_j}+q_{v_mj}+q_{e_j})+\frac{\partial}{\partial x_j}(u_i\tau_{ij}+\sum_s^{ns}(\rho_s h_s V_s^j))=\sum_s \epsilon N_s Z_s E_i u_i. \tag{3}$$

A vibrational energy equation for each nonequilibrium molecule,

$$\frac{\partial \rho e_{\mathrm{v}_m}}{\partial t}+\frac{\partial}{\partial x_j}(\rho e_{\mathrm{v}_m}u_j)+\frac{\partial}{\partial x_j}(q_{v_mj}+\rho e_{\mathrm{v}_m}V_m^j)=Q_{\mathrm{T-v}_m}\hat{M}+Q_{\mathrm{v-v}_m}+Q_{\mathrm{v}_m\mathrm{-e}}. \tag{4}$$

An electron–electronic energy equation,

$$\frac{\partial \rho e_\mathrm{e}}{\partial t}+\frac{\partial}{\partial x_j}((\rho e_\mathrm{e}+p_\mathrm{e})u_j)+\frac{\partial}{\partial x_j}(q_{e_j}+\sum_s \rho_s e_{e_s}V_s^j)=u_j\frac{\partial p_\mathrm{e}}{\partial x_j}-Q_{\mathrm{v}_m\mathrm{-e}}+Q_{\mathrm{T-e}}+Q_\mathrm{el}. \tag{5}$$

The electronic states of each species are characterized by Boltzmann distribution at T_e (Tchuen et al., 2005). The absence of the conduction current is assumed, and an induced electric field due to the presence of electron in the flow is expressed as

$$\vec{E} \simeq -\frac{1}{N_e \epsilon}\vec{\nabla} p_e. \tag{6}$$

The mixture is assumed to be electrically neutral ($\sum_s \epsilon N_s Z_s E_i \simeq 0$) as a consequence of the chemical kinetic mechanism; for each NO^+ ion produced/consumed in the flow, an electron is also produced/consumed. The local charge neutrality is also assumed. Thus, the number of electrons is equal to the number of ions at each point:

$$\rho_e = \hat{M}_e \sum_{s=\text{ions}} \frac{\rho_s}{\hat{M}_s}. \tag{7}$$

The state equation of the gas allows to close the system of Eqs. (1) to (5). The total pressure is given as the sum of partial pressures of each species regarded as perfect gas

$$p = \sum_{s=1}^{NS} p_s = \sum_{s\neq e} \rho_s \mathscr{R}_s T + \rho_e \mathscr{R}_e T_e. \tag{8}$$

The total energy of the mixture per unit volume

$$\rho e = \sum_{s\neq e} \rho_s C^s_{v,\text{tr}} T + \frac{1}{2}\sum_s \rho_s u_s^2 + \sum_{m=1}^{NM} \rho_m e_{v_m} + \rho e_e + \sum_{s=1}^{NS} \rho_s h_s^0. \tag{9}$$

is splitted between the translational–rotational, kinetic, vibrational, electron–electronic contributions, and the latent chemical energy of the species. T and T_e are deduced through Eqs. (5) and (9) with an iterative method. The vibrational temperature of the diatomic species m is determined by inverting the expression for the energy contained in a harmonic oscillator at temperature T_{v_m}:

$$e_{v_m} = \frac{\mathscr{R}}{\hat{M}_m}\frac{\theta_{v,m}}{e^{\theta_{v,m}/T_{v_m}} - 1}. \tag{10}$$

2.1. Transport coefficients

The viscous stresses τ_{ij} are defined with the hypothesis of Stokes. The dynamic viscosity is given by Blottner et al. (1971) interpolation law. The thermal conductivity of each species is derived from Vincenti and Kruger's (1965) relation. Wilke's semi-empirical mixing rule (Wilke, 1950) is used to calculate total viscosity and conductivity of the gas. For simplicity, the mass diffusion fluxes for neutral species are given by Fick's law with a single diffusion coefficient (Tchuen et al., 2005). The diffusion of ions is modeled with ambipolar diffusion coefficient $D_{\text{ion}}^{\text{ambi}} = 2D_s$. To improve this formula, we used $D_{\text{ion}}^{\text{ambi}} = D_{\text{ion}}(1 + T_e/T)$ as recommended in Josyula and Bailey (2003); Ramsaw and Chang (1993). The effective diffusion coefficient of the electrons (D_e) is proportional to the ambipolar diffusion coefficient of the ions (Tchuen et al., 2005).

The total heat flux is assumed to be given by Fourier's law as

$$Q = \sum_s q_s = -\sum_s (\lambda_{\text{tr},s}\nabla T + \lambda_{v,s}\nabla T_{v,s} + \lambda_{\text{el},s}\nabla T_e + \rho D_s h_s \nabla Y_s). \tag{11}$$

which is the resultant of the flux of conduction, vibration, electronics and the diffusion of the total energy. After using an extension form of Masson and Monchick assumptions (1962), and the relation given by Ahtye (1972) to connect thermal conductivity of vibration with the diffusion coefficient, a more convenient form of the total heat flux is obtained as in Tchuen et al. (2005).

2.2. Energy exchange model

The energy exchange between translation and vibrational mode Q_{T-v} is described according to Landau–Teller theory (Park, 1990)

$$Q_{T-v_m} = \rho_m \frac{e_{v_m}(T) - e_{v_m}(T_{v_m})}{\tau_m} \tag{12}$$

and τ_m is the relaxation time expressed as in Tchuen et al. (2005).

The vibrational energy transfer between the different molecules is modeled by Candler and MacCormarck (1991):

$$Q_{v-v_m} = \sum_{s\neq m} P_{sm} Z_{sm} \frac{\hat{M}_s}{\mathscr{N}}[e_{vs}(T_{vsm}) - e_{vs}], \tag{13}$$

where T_{vsm} is the same vibrational temperature obtained after the collision of the two molecules, Z_{sm} is the $s-m$ collision number per unit volume which is determined from kinetic theory (Vincenti and Kruger, 1965), P_{m-s} and P_{s-m} are the two probabilities originating from the work of Taylor et al. (1967). These probabilities have been presented recently in an exponential form by Park and Lee (1993).

The expression of the energy exchanged during electron-heavy particles collisions is derived from Lee (1985)

$$Q_{T-e} = 3\mathscr{R}\rho_e(T - T_e)\sqrt{\frac{8\mathscr{R}T_e}{\pi M_e}}\sum_{r\neq e}\frac{\rho_r N}{\hat{M}_r^2}\sigma_{er}, \tag{14}$$

where σ_{er} are the collision cross-sections for interaction electron-other particle. The value is assumed to be constant and equal to 10^{-20} m^2.

Q_{e-v_m} is the energy source term from vibration–electron coupling. It is assumed that only N_2–e coupling is strong (Lee, 1986), and its expression is assumed to be of the Landau–Teller form:

$$Q_{e-v_m} = \rho_m \frac{\hat{M}_m}{\hat{M}_e}\frac{e_{v_m}(T_e) - e_{v_m}(T_{v_m})}{\tau_{em}}; \quad m = N_2. \tag{15}$$

where the relaxation time τ_{em} is a function of electron–electronic temperature and electron pressure as presented in Candler and MacCormarck (1991). The term Q_{el} accounts for the rate of electron energy loss when a free electron strikes a neutral particle and ionizes it, with a loss in electron translational energy.

2.3. Chemistry model

The chemical reactions model used is proposed by Park (1985) which is applied to seven air species (O, N, NO, O_2, N_2, NO^+, e^-) with 24 elementary reactions. The primary chemical reactions considered between species are

$$\begin{aligned}
&O_2 + M \rightleftharpoons O + O + M,\\
&N_2 + M \rightleftharpoons N + N + M,\\
&NO + M \rightleftharpoons N + O + M,\\
&O + N_2 \rightleftharpoons NO + N,\\
&NO + O \rightleftharpoons O_2 + N,\\
&N + O \rightleftharpoons NO^+ + e^-,
\end{aligned}$$

where the catalytic species M stands for any of the seven species. The mass production rate is governed by the forward and backward reaction rate constants defined by

$$K_{f,r}(T_a) = A_r T_a^{\alpha_r}\exp(-\theta_r/T_a), \tag{16}$$

$$K_{b,r}(T) = \frac{K_{f,r}(T)}{K_{eq,r}(T)}. \tag{17}$$

The equilibrium constant $K_{eq,r}$ is usually given as a function of temperature:

$$K_{\mathrm{eq,r}} = \exp\left(\sum_{i=1}^{5} A_{\mathrm{ir}} Z^{i-1}\right), \quad Z = \frac{10,000}{T}. \tag{18}$$

The constants A_{ir}, A_{r}, α_{r}, and θ_{r} are experimentally determined and can be found in Park (1985). The vibration–dissociation coupling (CVD) for diatomic species is modeled according to the empirical relationship suggested by Park (1990) with the definition of the average temperature T_{a}. The controlling temperature T_{a} of different reactions is defined here as a weighted average of the translational temperature T of heavy particle and vibrational temperature T_{v_m} when no free electrons are generated. Thus, for the dissociation reactions, $T_{\mathrm{a}} = T^{q} T_{\mathrm{v}_m}^{1-q}$ is used in the forward reactions while the backward reactions are controlled by $T_{\mathrm{a}} = T$. When the impacting particle is an electron, the forward rate is controlled by vibrational and electron temperatures. Sharma et al. (1988) suggested that the value of q varied from 0.6 to 0.7 might be more realistic especially for highly energetic flows, and the value 0.7 is chosen here.

3. Numerical method

3.1. Numerical procedure

The governing partial differential Eqs. (1) to (5) are discretized in space by using a finite-volume approach with a central formulation over structured mesh. The inviscid fluxes at cell interfaces are calculated through a Flux-Difference-Splitting (FDS) approach which uses the solution of the local Riemann problem (Godunov, 1959). The second-order spatial accuracy is obtained by employing the monotonic upstream schemes for conservation laws (MUSCL-Hancock) (Roe, 1983) with a TVD extension type scheme approach. The exact Riemann solver is replaced by an AUSM+ in the case of a strong shock wave, and the Mimmod limiter function is used for the inviscid fluxes. The viscous terms are classically discretized by second-order central difference approximation.

The explicit formulation, which gives the variation of $U_{i,j}$ during time Δt on each cell (i,j), can be written in two-dimensional axisymmetric coordinate as

$$\frac{\Delta U_{i,j}}{\Delta t} + \frac{1}{A_{i,j} r_{i,j}^{\alpha}} \sum_{k=1}^{4} F_k N_k = \alpha H_{i,j} + \Omega_{i,j}, \tag{19}$$

where $\alpha = 1$ for an axisymmetry coordinate system, and $\alpha = 0$ for planar two dimensions. This equation, extended to all domain, allows the numerical computation of all unknown variables of the system for unsteady flowfield. The source term Ω is treated implicitly to relax the stiffness. A time predictor–corrector algorithm is used to obtain second-order time accuracy. The speed of sound plays a major role in flux-split algorithm. Its evaluation in the case of one translational temperature is no longer applicable in the case of multiple translation temperature. The correction of the speed of sound due to electronic contribution and the presence of electron translational temperature has been included (Cinnella and Grossman, 1990):

$$a^2 = \gamma\left(\frac{p}{\rho}\right) + (\gamma - 1)\left(\frac{T}{T_{\mathrm{e}}} - 1\right)\frac{p_{\mathrm{e}}}{\rho}, \tag{20}$$

where classical speed of sound is obtained when $T = T_{\mathrm{e}}$.

The structure of this code is multi-blocks, and uses parallel processing machine architecture for significant enhancement of efficiency in treating of complex flow configuration. A detailed description of this numerical method may be found in Tchuen et al. (2005).

3.2. Boundary conditions

The freestream condition is hypersonic. The outflow is supersonic, and the zero gradient exit condition is appropriate. Along the stagnation line, the flowfield is symmetric. The wall temperature (T_{w}) is fixed, and zero normal pressure gradient is imposed. The no-slip and no-temperature jump conditions are used. At the wall, the flow is generally assumed to be in thermal equilibrium. Because of the shielding effect, we have assumed either $T = T_{v_s} = T_{\mathrm{e}}$ when vibrational and electronic energy content is greater than the electron translational energy content or $\partial T_{v_s}/\partial n = \partial T_{\mathrm{e}}/\partial n = 0$ otherwise. The wall is supposed to be chemically noncatalytic.

The upstream flow conditions and the details of grid considered in this study are reported in Table 1. In each case, the freestream air gas is composed of 79% N_2 and 21% O_2. The gas rarefaction, which is characterized with the Knudsen number, is related to Mach number and Reynolds number

$$Kn_{\infty} = \frac{Ma}{Re}\sqrt{\gamma\frac{\pi}{2}}; \quad Re_{\infty} = \frac{R U_{\infty} \rho_{\infty}}{\mu}, \tag{21}$$

where R is the radius. The grid point used in calculations is densely distributed near the wall and near the shock standoff distance as shown in Fig. 1. The number of nodes and the minimum grid spacing in x and y directions, respectively, are reported in Table 1.

Table 1
Detail of freestream conditions and grids used for RAM CII Calculation

Experiments	Ram CII Candler and MacCormarck (1991)	Ram CII Candler and MacCormarck (1991)
Altitude (km)	61	71
R (mm)	152.4	152.4
M_{∞}	23.9	25.9
U_{∞} (m/s)	7636.4	7658.6
P_{∞} (P_{a})	19.85	4.764
T_{∞} (K)	254	216
T_{w} (K)	1500	1500
$R_{e_{\infty}}$	19,500	6280
$K_{n_{\infty}}$	1.2×10^{-3}	4.1×10^{-3}
Grid IM	60	70
Grid JM	70	70
$\Delta x_{\min}$(m)	2.1172×10^{-5}	2.002×10^{-5}
$\Delta y_{\min}$(m)	2.7318×10^{-4}	1.27×10^{-4}

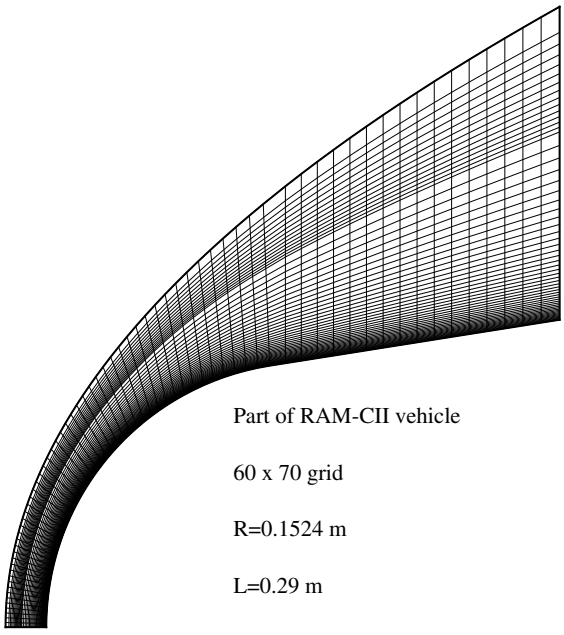

Fig. 1. Computational grid 60 × 70 for a part of RAM-C.

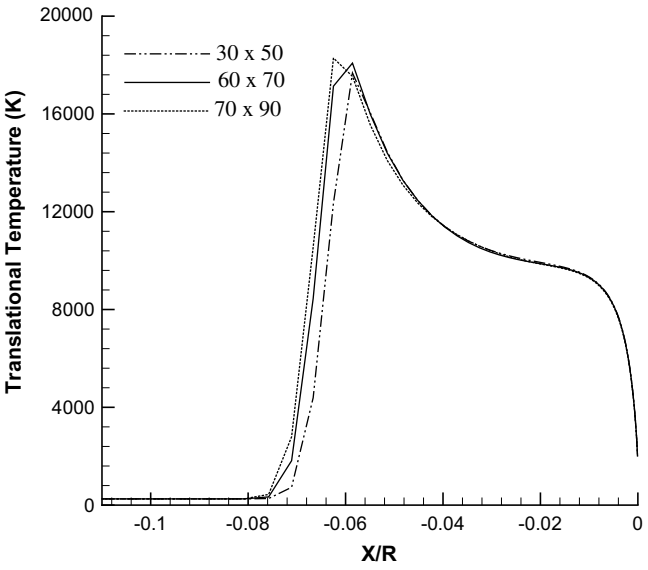

Fig. 2. Grid independence: temperature along stagnation line; Mach 23.9.

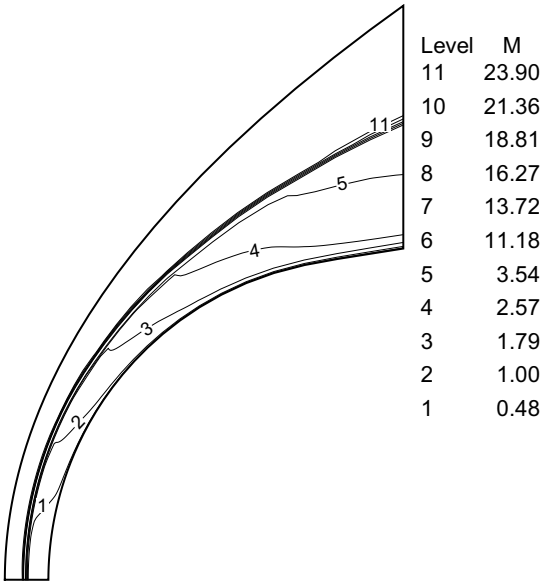

Fig. 3. Mach number contours for RAM-C at 61 km.

Three grid levels have been employed to achieve grid independence. For the Mach 23.9 case, the following grid sizes (30×50), (60×70) and (70×90) are used. The effect of the grid sizes on the translational temperature distribution and the shock detachment distance along the stagnation streamline is shown in Fig. 2. The coarse grid of 30×50 nodes has a lower translational temperature than the medium grid 60×70 and the fine grid of 70×90 grid. The shock wave is better represented by the medium and fine grids. The magnitude of the Richardson extrapolation error estimator (Roache, 1998) for the peak translational temperature using the coarse and medium grids is 2.85%, and using the medium and the fine grids is 1.30%. The medium grid with 60×70 nodes in the axial and normal directions, respectively, was considered adequate, and used for the Mach 23.9 case. A similar grid study conducted for the Mach 25.9 case resulted in the use of 70×70 nodes in the axial and normal directions.

4. Results and discussions

The numerical results presented here concern Radio Attenuation Measurement RAM-C tests. The figure of flight experiments is shown in Park (1990). The RAM-C flight is a program conducted by the NASA Langley Research Center to assess the effects of blackout during re-entry. The body for each RAM-C flight was a blunted sphere–cone with a 0.1524 m nose radius, 9-deg cone half-angle, and a total length of 1.3 m. Two cases of Mach 23.9 and 25.9 corresponding, respectively, at altitudes of 61 km and 71 km are studied here. The RAM-C experiment is chosen for its boundary conditions which are perfectly definable. The computations were performed to replicate the RAM C-II flight experiment and to confirm the capacity of the code to simulate correctly weakly ionized hypersonic flow. These experiments were numerically studied by several authors (Candler and MacCormarck, 1991; Park, 1990; Josyula and Bailey, 2003; Barbante, 2001). The interest of different works is to highlight a model that produces better results. The influence of the reel gas effect on aerothermodynamic parameters is investigated here.

4.1. The $M_\infty = 23.9$ case, $H = 61$ km

The contours Mach number are plotted in Fig. 3, and show the strong detached bow shock wave with a subsonic pocket in the nose region. The shock wave converts the high kinetic energy of the upstream flow into the various internal energy modes, leading to significant chemical and thermal nonequilibrium in the stagnation region. The contours pressure isolines are drawn in Fig. 4. The thickness of the shock layer is visible and enables the appreciation of the position and the intensity of the shock. The peak pressure occurs at the stagnation point in the compression zone, and decreases rapidly as the gas expands along the body. Fig. 5 shows the predicted temperature distribution obtained along the stagnation streamline at Mach 23.9. The comparative evolution of the various temperatures justifies the choice of the model at four temperatures. The difference between $T_{v_{O_2}}$ and $T_{v_{N_2}}$ becomes larger for a strong Mach number in a flow at relatively low density condition. The use of a model at one temperature of vibration can induce miscalculations in the kinetic of the reactions, which will influence the calculation of the thermodynamic parameters. The mass fractions of the major constituents of the gas on the stagnation line are plot-

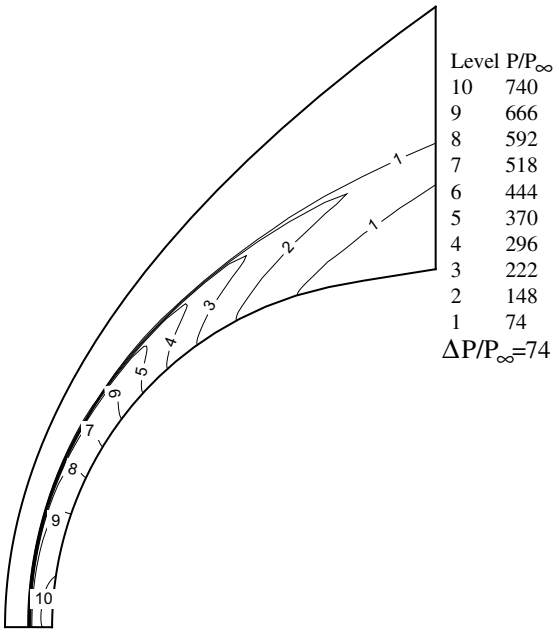

Fig. 4. Pressure contours; Mach 23.9.

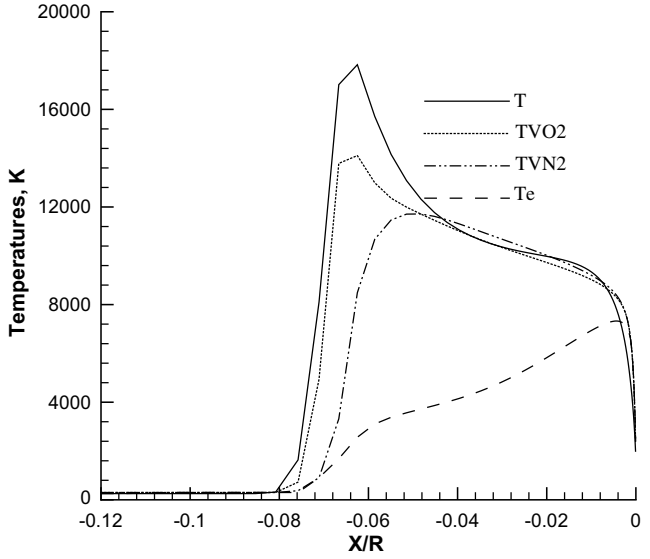

Fig. 5. Temperatures distribution along the stagnation line for RAM-C at 61 km.

ted in Fig. 6. The relatively high density conditions of the flow yield a high reactivity. The oxygen is fully dissociated. This plot indicates the degree of chemical nonequilibrium in the flowfield. Behind the shock wave, the molecules of oxygen are completely dissociated, and one notes a strong recombination of diatomic nitrogen near the wall because of the relatively cooled wall which does not favor the dissociation.

Fig. 7 shows the same quantities at the point where the sphere, and the cone join. At this location, the flow is supersonic except in the boundary layer and the gas that originated at the nose has expanded around the sphere causing the translational temperature to drop. As a result, the gas is less reactive. The oxygen in the wall region is fully dissociated and the nitrogen is appreciably reacted. The maximum concentration of NO^+ and e^- is less than 0.02%, and is not drawn here. This is due to the strong expansion of the flow, which causes the freezing of the vibrational-electron–electronic excitation energy. Fig. 8 shows that the gas is relatively cool with a peak translational–rotational temperature of 7500 K. The

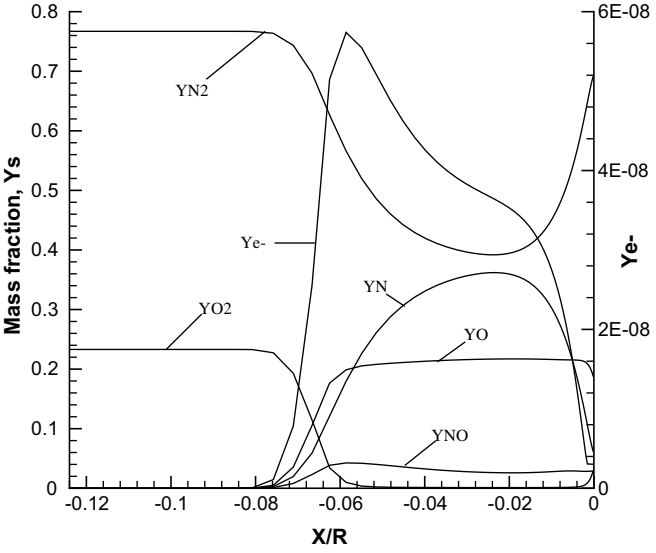

Fig. 6. Mass fraction along the stagnation line, $M_\infty = 23.9$.

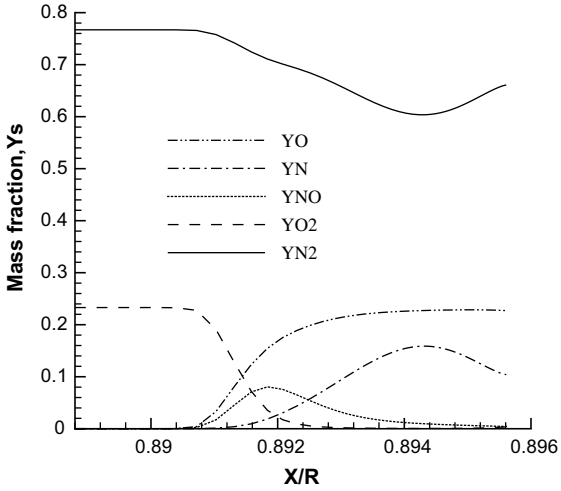

Fig. 7. Mass fraction at $Y/R = 1$ position, Mach 23.9.

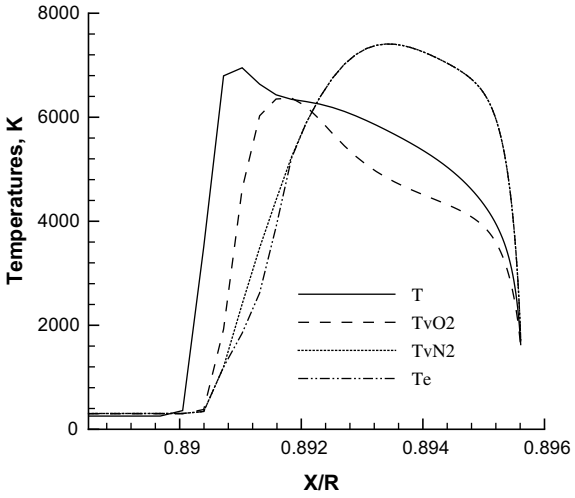

Fig. 8. Temperatures at $Y/R = 1$ position, Mach 23.9.

vibrational temperature of N_2 is higher than the translational temperature near the wall. The identical evolution of T_e and $T_{v_{N_2}}$ shows the strong coupling which exists between N_2 and e^-. This is a result of the vibrational temperature energy being frozen in the gas as it is swept around the shoulder of the body. The equilibration of N_2 vibrational temperature and electronic temperature is the basis of Park's two-temperature model.

The non-dimensional standoff distance, the peak temperatures $(T, T_{v_{N_2}})$ and NO^+ peak mass fraction are compared to those obtained with the computational codes implemented by other authors as shown in Table 2. The peak of translation–rotational

Table 2
Comparison code to code along the stagnation line for RAM-CII at $M_\infty = 23.9$

Parameters	Present	Candler and MacCormarck (1991)	Josyula and Bailey (2003)	Coquel and Marmignon (1997)
$\delta = X/R$ (%)	6.75	9.18	7.21	7.87
Peak of T (K)	18,400	22,500	20,500	20,000
Peak of $T_{v_{N_2}}$ (K)	11,700	11,000	9400	13,000
Peak of T_e (K)	8025	8300	8700	–
Peak of NO^+ (%)	0.313	0.164	0.1	0.32

temperature reaches 18,400 K. The electron temperature peak near the wall is about 8025 K, and is closed to the temperature obtained by Candler and MacCormarck (1991). The last excited mode is electronic mode. Various existing couplings lead to a relaxation of all internal modes towards the wall temperature. The dispersion observed can be attributed to the difference in the models despite some commonalities among them. Candler and MacCormarck (1991) used an implicit Gauss Siedel line relaxation technique developed by MacCormack, with a coarse mesh for calculation. Josyula and Bailey (2003) included additional eigenvalue in flux splitting, Roe flux difference split scheme with an entropy correction is used. Coquel and Marmignon (1997) used the Roe scheme.

The skin friction coefficient ($\tau_w/(\frac{1}{2}\rho_\infty U_\infty^2)$) and the wall heat flux are plotted in Figs. 9 and 10. One notes a sensitive decay of maxima of friction coefficient with the consideration of the electronic relaxation. By neglecting these effects, the chemical reaction will be overestimated. In the compression zone, the influence of the normal gradient is clearly evident and past the compression zone, the longitudinal velocity gradient at the wall is high. One can notice that the electronic thermal contribution affects the surface heat flux with an increase of about 8.6% at the stagnation point. Barbante's stagnation point heat flux is also reported. Barbante (2001) uses the Hybrid Upwind Splitting (HUS) scheme with a seven species air model.

4.2. The M_∞ = 25.9 case, H = 71 km

The predicted temperature distribution along the stagnation streamline is shown in Fig. 11 for Mach 25.9 case. When one takes into account the electronic excitation, a new distribution of energies on the internal modes is obtained. The evolution of various temperatures is different. The peak of translational temperature is around 19,900 K behind shock wave. This high temperature leads to an important chemical activity. Fig. 12 shows the resulting mass concentrations of species along the stagnation streamline. Oxygen is fully dissociated behind the shock wave, and nitrogen molecules are dissociated with a mass fraction of 0.56 near the surface. For a high Mach number air flow, the dissociation products of nitrogen and oxygen downstream of the shock recombine to form nitric oxide molecules which ionize at the high temperatures. Free electrons are produced in the flowfield in the associative-ionization reaction of nitric oxide. The formation of the peak of the electrons is at the normalized location (X/R_n) of 0.05 in the postshock region. This maximum corresponds with the maxima of NO^+ concentration.

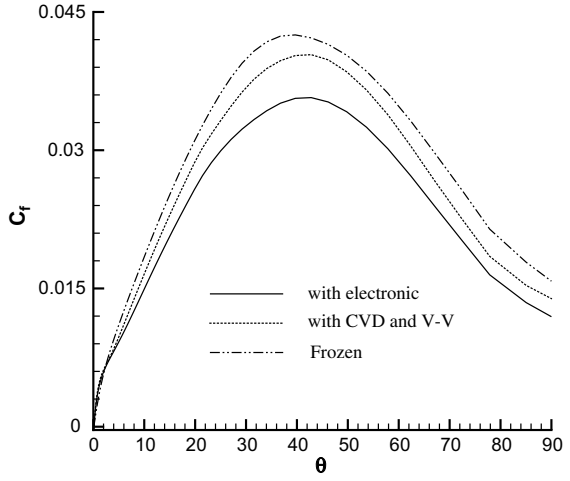

Fig. 9. Influence of electronic relaxation on the skin friction coefficient for Mach 23.9.

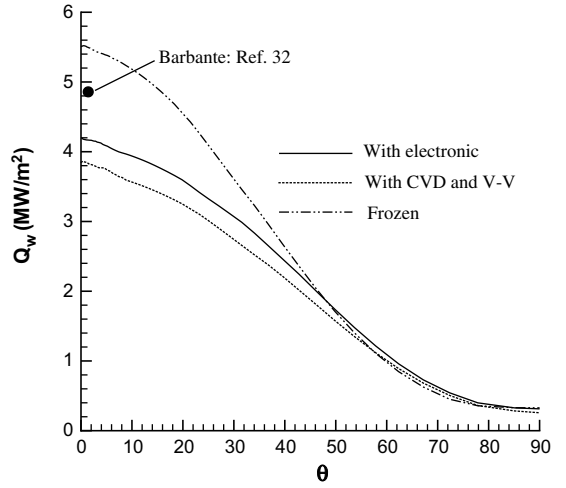

Fig. 10. Influence of electronic relaxation on the wall heat flow for Mach 23.9.

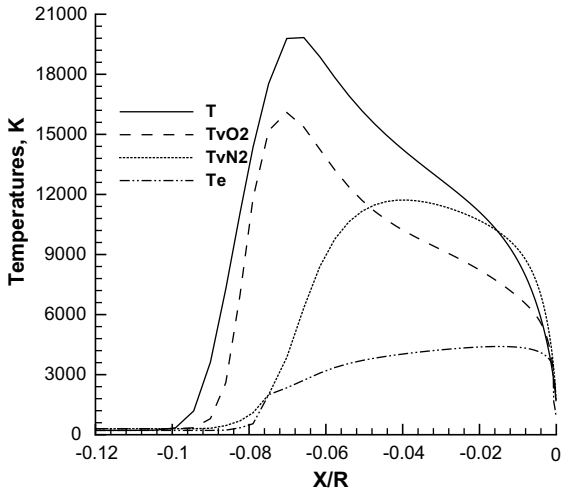

Fig. 11. Temperatures evolution along the stagnation line; Mach 25.9.

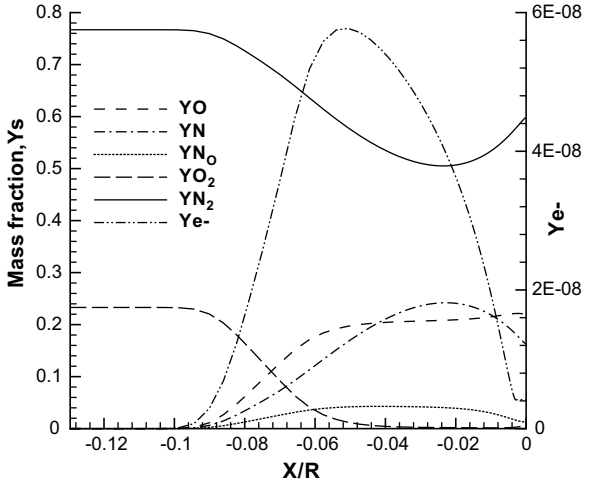

Fig. 12. Mass fraction evolution along the stagnation line; Mach 25.9.

Table 3
Comparison code to code along the stagnation line for RAM-CII at $M_\infty = 25.9$

Parameters	Present	Candler and MacCormarck (1991)	Josyula and Bailey (2003)
$\delta = X/R$ (%)	8.47	12.46	9.84
Peak of T (K)	19,900	25,000	22,000
Peak of $T_{v_{O_2}}$ (K)	16,000	10,700	–
Peak of $T_{v_{N_2}}$ (K)	11,750	11,000	13,500
Peak of T_e (K)	4510	6500	5100

A very good comparison of some aerothermodynamics parameters is presented in Table 3. Candler and MacCormarck (1991) and Josyula and Bailey (2003) results are also reported. Substantial discrepancies can be observed between the different results obtained. The wide dispersion obtained in the table comes from the different models used by the authors cited. One can also observe that for Mach 23.9 case, the nonequilibrium effects are confined to about half the shock layer. As a consequence, the standoff distance increases by approximately 20.31% than Mach 25.9 case.

The comparison of the friction coefficient and wall heat flux is drawn in Figs. 13 and 14. One notes a decrease of maxima of the friction coefficient of the order of 6.12% and an increase of about 9.16% of the stagnation point heat transfer during the consideration of the electronic relaxation. Candler and MacCormarck (1991) have also performed calculations with an air-7 model derived from Park, with fixed temperature and noncatalytic wall boundary conditions. As shown Fig. 14, the predicted heat flux at the stagnation point obtained by Candler and MacCormarck (1991) and estimated from Stanton number is about 2.5 MW/m^2. Figs. 10 and 14 show the interest to take into account all modes of energy in the calculation of heat flux. The influence of chemical reactions which are endothermic is also perceptible.

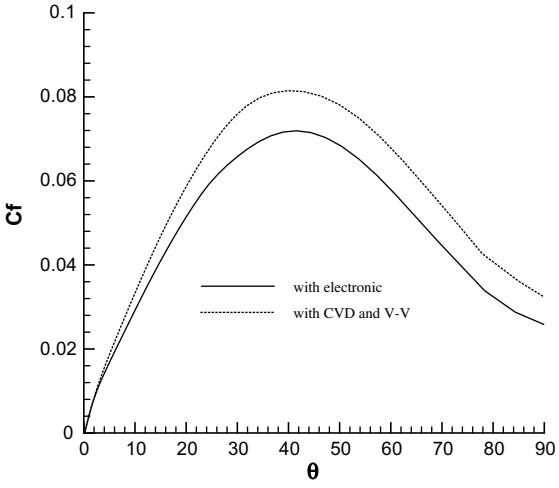

Fig. 13. Influence of electronic relaxation on the skin friction coefficient for Mach 25.9; $H = 71$ km.

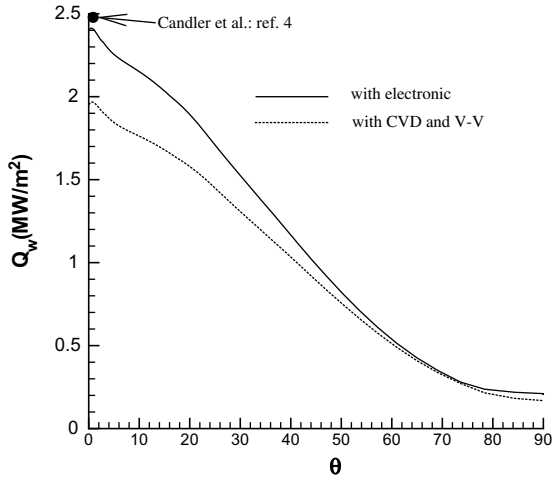

Fig. 14. Influence of electronic relaxation on the wall heat flow for Mach 25.9; $H = 71$ km.

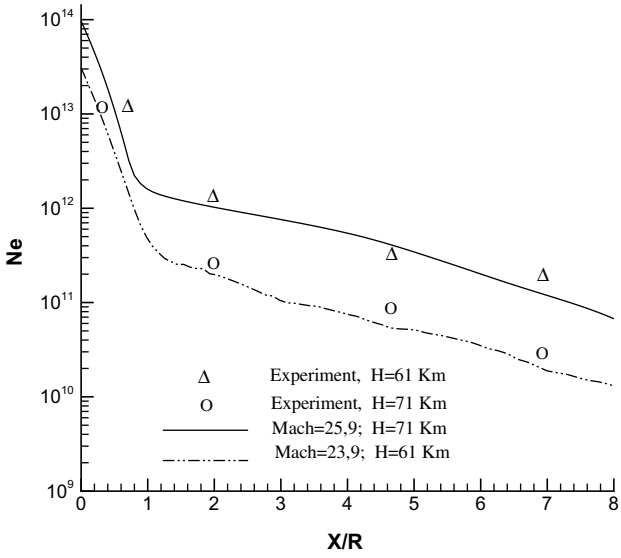

Fig. 15. Comparison with experiment of the peak of electron number density following the axial distance.

Fig. 15 shows the comparison of the computed and the measured peak electron number density along the body for Mach 23.9 and 25.9. The comparison shows very good agreement, with a scatter from the experimental values similar to that reported by other authors. Most of the ionization occurs at stagnation region. The electron number density is maximal in the stagnation point of the obstacle, and decreases along the body.

5. Conclusion

Application of the model to compute flow such as Radio Attenuation Measurement Experiment (RAM-C) shows reasonably accurate solutions. The present mathematical and numerical model allowed a robust, and efficient code to be developed, leading to a better evaluation of various aerothermodynamic parameters for high Mach numbers. The results were successfully validated with experimental and computation work for surface heat transfer, the shock standoff distance and thermodynamic parameters.

The effect of electronic relaxation and ionization on temperature distributions and species concentrations is noticeable. Stagnation point heat flux for the solution with electronic relaxation is 4–9.2% higher than for the solution without electronic nonequilibrium according to considered cases. To neglect these effects in high enthalpy flow can lead to an overestimation of chemical activities and an underestimation of the wall heat flux.

Further research is required for the development of the numerical algorithm which will improve the computational time that remains very long. An improvement of the present model should envisage an extension of the number of chemical species that would allow for the consideration of the radiation in the flowfield.

References

Ahtye, W.F., 1972. Thermal conductivity in vibrationally excited gases. Journal of Chemical Physics 57, 5542–5555.

Appleton, J.P., Bray, K.N.C., 1964. The conservation equations for a nonequilibrium plasma. Journal of Fluid Mechanics 20 (4), 659–672.

Barbante, P.F., 2001. Accurate and efficient modelling of high temperature nonequilibrium Air flows. Ph.D. Thesis, Université Libre de Bruxelles.

Blottner, F.G., Johnson, M., Ellis, M., 1971. Chemically Reacting Viscous Flow Program for Multi-Component Gas Mixtures. Sandia Laboratories, Albuquerque, NM, Report. Sc-RR-70-754.

Candler, G.V., MacCormarck, R.W., 1991. Computation of weakly ionized hypersonic flows in thermochemical nonequilibrium. Journal of Thermophysics and Heat Transfer 5 (3), 266–273.

Cinnella, P., Grossman, B., 1990. Upwind Technique for flow with multiple translational temperatures. AIAA-90-1660, Seattle,WA.

Coquel, F., Marmignon, C., 1997. Simulation numérique d'écoulements en déséquilibre thermochimique et faiblement ionisés. ONERA Rapport Technique de Synthése TRS 14/1929 AY.

Gnoffo, P.A., Gupta, R.N., Shinn, J.L., 1989. Conservation Equation and Physical Models for Hypersonic Air flows in Thermal and Chemical Nonequilibrium, NASA Technical Paper 2867.

Godunov, S., 1959. A difference scheme for numerical computation of discontinuous solution of hydrodynamic equations. Mathematics of the USSR-Sbornik 47, 271–306.

Josyula, E., Bailey, F.W., 2003. Governing equations for weakly ionized plasma flowfields of aerospace vehicles. Journal of Spacecraft and Rockets 32 (6), 845–857.

Lee, J.-H., 1985. Basic governing equations for the flight regimes of aeroassisted orbital transfer vehicles. In: Thermal design of aeroassisted orbital transfer vehicles. In: Nelson, H.F. (Ed.), . Progress in Astronautics and Aeronautics, vol. 96. American Institute of Aeronautics and Astronautics, Inc., pp. 3–53.

Lee, J.-H., 1986. Electron-impact vibrational excitation rates in the flowfield of aeroassisted orbital transfer vehicle. In: Moss, J.N., Scott, C.D. (Eds.), Progress in Aeronautics and Astronautics. Thermophysical Aspect of Re-entry Flow, vol. 103. AIAA, New York, pp. 197–224.

Luneau, J., Rossines, P., 1978. Aérodynamique hypersonique – Le phénoméne de black-out. Ecole Nationale Supérieure de L'Aéronautique et de l'Espace.

Masson, E.A., Monchick, L., 1962. Heat conductivity of polyatomic and polar gases. The Journal of Chemical Physics 36 (6), 1622–1640.

Mitcheltree, R.A., 1991. A parametric study of dissociation and ionization models at 12 km/s. AIAA Paper 91-1368.

Palmer, G., 1989. The development of an explicit thermochemical nonequilibrium algorithm and its applications to compute three dimensional AFE flowfields. AIAA Paper 89-1701.

Park, C., 1985. On convergence of computation of chemically reacting flows. AIAA Paper 85-0247.

Park, C., 1990. Nonequilibrium Hypersonic Aerothermodynamics. Wiley, New York.

Park, C., Lee, S.-H., 1993. Validation of multitemperature nozzle flow code NOZNT. In: AIAA 28nd Thermophysics Conference, Orlando, FI. AIAA Paper 93-2862.

Ramsaw, J.D., Chang, C.H., 1993. Ambipolar diffusion in two temperature multicomponent plasma. Plasma Chemistry and Plasma Processing 13 (3), 489–498.

Roache, P., 1998. Verification and validation in computational science and engineering. Hermosa, Albuquerque, NM. pp. 107-142.

Roe, P., 1983. Approximate Riemann solvers, parameters vectors and difference schemes. Journal of Computational Physics 43, 357–372.

Sharma, S.P., Huo, W.M., Park, C., 1988. The rate parameters for coupled vibration–dissociation in a generalized SSH approximation flows. AIAA-88-2714.

Taylor, R., Camac, M., Feinberg, M., 1967. Measurement of vibration–vibration coupling in gas mixtures. In: Proceedings of the 11th International Symposium on Combustion, Pittsburg, PA, pp. 49–65.

Tchuen, G., Burtschell, Y., Zeitoun, E.D., 2005. Numerical study of nonequilibrium weakly ionized air flow past blunt body. International Journal of Numerical Methods for Heat and Fluid Flow 15 (6), 588–610.

Vincenti, W.G., Kruger Jr., C.H., 1965. Introduction to Physical Gas Dynamics. Wiley, New York.

Wilke, C.R., 1950. A viscosity equation for gas mixture. Journal of Chemical Physics 18 (4), 517–519.